

THERMODYNAMIC AND MECHANICAL MODELS OF INTERFACIAL EMBRITTLEMENT

PETER M. ANDERSON¹, JIAN-SHENG WANG²,
and JAMES R. RICE²

¹ Department of Materials Science and Engineering, Ohio State University, Columbus, Ohio, 43210

² Division of Applied Sciences, Harvard University, Cambridge, MA 02138

ABSTRACT

We present thermodynamic and mechanical models of interfacial embrittlement. These include consideration of the dependence of interfacial decohesion on segregants and their mobility, and analysis of the competition between cleavage decohesion and dislocation blunting at an interfacial crack tip. Results are illustrated by applications to various segregants (H, C, P, Sn, Sb, S) in Fe with estimates of their effects on the work of interfacial decohesion, $2\gamma_{\text{int}}$. The theory on emission versus cleavage is applied to the model system of [110] symmetric tilt Cu bicrystals with segregated Bi. Two of those and other Cu bicrystals were grown, heat treated, and tested mechanically. The [110] tilt bicrystals show qualitative compatibility with the theory, which could not be closely tested. As a group, the bicrystals showed highly variable resistance to interfacial cracking and a range of fracture morphologies.

INTRODUCTION

We review some thermodynamics and mechanics concepts used to study intergranular decohesion and the embrittlement or toughening caused by interface impurity segregants. The discussion first focuses on elastic-brittle fracture, and considers the Griffith condition for a cracking interface on which an impurity segregant lies. Using a thermodynamic framework that includes both adsorption and decohesion, the general features which distinguish cohesion enhancers from reducers are noted. Quantitative estimates are made of the deleteri-

ous effects of P, Sn, Sb, S and H on Fe grain boundaries and of why C seems to moderate the embrittling effects of such segregants.

Crack tip dislocation interactions may relax the high crack tip stress field and/or blunt a sharp crack tip, and therefore determine whether an atomically-brittle decohesion mode will occur. This issue is addressed in the context of a critical set of elastic stress intensity factors, K_M^{disl} ($M = 1, 2, 3$ denotes the loading mode), for emission of a single dislocation from a crack tip. Whether such emission or, instead, atomic decohesion occurs first as a stationary crack tip is loaded is regarded as fundamental to whether a cracked crystal, or interface, is intrinsically cleavable. Some qualifications to exercising this criterion are that the effect of external dislocations not nucleated from the crack tip and the overall viscoplastic dynamics of crack propagation are not accounted for in the present model.

The effect of a driving force for impurity segregation to the dislocation core or blunted crack tip will generally be to reduce the critical crack tip loading for dislocation emission from the impurity-free value. A successful embrittler must, however, reduce the critical crack tip load for cleavage below both that for crack tip dislocation emission and that for extensive nucleation and motion of external, non-crack-tip dislocations.

Finally, the work of atomically-brittle decohesion is evaluated for several Cu-Bi [110] symmetrical tilt interfaces, and is compared to corresponding estimates for dislocation emission from an interface crack. The work of decohesion is estimated to vary by up to 40% among the boundaries considered, and to reduce by up to 35% from the values for pure Cu. The corresponding value of energy release rate G for dislocation emission is expected to be little affected by impurities with low mobility such as Bi, at least assuming that residual elastic misfit stresses are small, although it is predicted to be highly dependent on the mode of crack loading and crack orientation.

Mode 1 tests of interfacial cracks in Cu-Bi bicrystals lead to ductile and brittle interface failure that is qualitatively consistent with theoretical predictions. Results include a dependence of brittleness on crack growth direction, as predicted theoretically, although it seems unlikely that the theoretical predictions could be correct in detail in describing interfacial fracture in this system.

INTERFACIAL SEGREGATION AND WORK OF DECOHESION

In this section, we first summarize recent discussions of interfacial segregation and cohesion by Rice (1) and Rice and Wang (2). Consider a loaded crack lying along an interface as shown in Fig. 1a. The criterion for crack growth in the absence of plasticity would be given by the Griffith condition,

$$G = 2\gamma_{\text{int}} \quad (1)$$

where G is the energy consumed per unit area of crack advance, and $2\gamma_{\text{int}}$ is the reversible work of separating the interface through displacement δ , against atomic cohesive forces as shown in Fig. 1a. If the tensile stress σ across the interface is regarded as a function of the crack profile displacement δ as shown in Fig. 1b, then

$$G = \int_0^{\delta'} \sigma(\delta) d\delta = 2\gamma_{\text{int}} \quad (2)$$

which one may recognize as the area under the σ versus δ curve. There may be other work modes involving in-plane shearing displacements which are not considered here. Rice and Wang (2) discuss various theoretical concepts for interfacial decohesion in non-ideally-brittle systems. They conclude that of those properties susceptible to alteration by atomic segregation of impurities to interfaces, the alterations of $2\gamma_{\text{int}}$ has an important but probably not exclusive role in determining embrittlement.

To evaluate the above integral relation for an interface containing an impurity (3,4), consider the interface as a thermodynamic system described in terms of Gibbsian excess quantities. For example, in a body loaded by remote uniform tension σ normal to the interface, define δ as the excess of total displacement of a point A in one phase relative to a point B in the other, over that accountable by homogeneous straining of the two phases in which points A and B reside. Then $\sigma d\delta$ is the excess of work over that accountable as work in straining the adjoining phases, and this work expression will obey the laws of thermodynamics in terms of analogously defined excess internal energy, heat adsorption, free energy (\bar{f} per unit area of undeformed interface), surface energy ($\bar{\gamma}$ per unit area of undeformed interface), entropy (\bar{s}), etc.

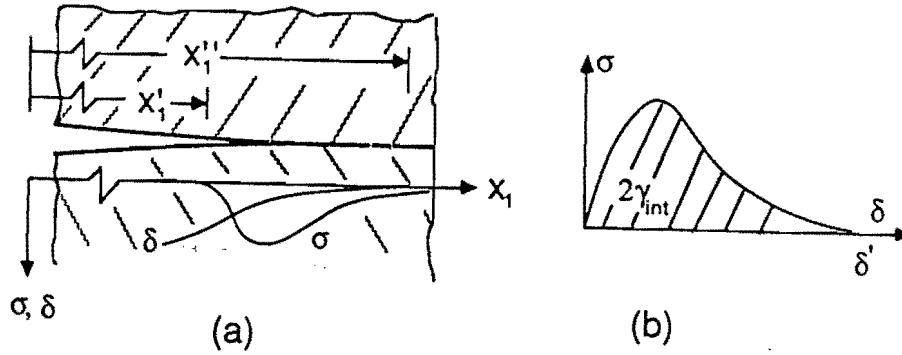


FIG. 1. (a). Loaded interfacial crack showing a schematic distribution of tensile stress σ and opening displacement δ at the crack tip. (b). Representation of the work of separation in the σ - δ plane.

A Constitutive Approximation for Local Interface Equilibrium

In fracture as affected by solute segregation, one is often concerned with interfaces that are out of composition equilibrium with the bulk, both before and after separation. For simplicity, a single segregant is considered which is present only at extremely small concentrations in the adjoining bulk phases so that the concentration Γ per unit reference area of interface is unambiguously defined. In order to deal with nonequilibrium separation, the constitutive approximation $\sigma = \sigma(\delta, \Gamma, T)$ and $\bar{f} = \bar{f}(\delta, \Gamma, T)$ is adopted. Within this approximation, the state functions, *e.g.*, $\bar{f}(\infty, \Gamma, T)$, are regarded as the same function of Γ irrespective of whether it refers to the energy of a pair of surfaces at temperature T that have been freshly created by a fracture and contain total solute Γ or to a pair of free surfaces which have reached a state of composition and reconstruction equilibrium at temperature T and solute content Γ . The model described by this approximation is thus one for which all states of the interface are at local equilibrium, but are not necessarily at equilibrium with the bulk phases.

By standard thermodynamic formalism, but assuming that the interface is constrained against composition equilibrium with the ad-

joining bulk phases,

$$\begin{aligned} d\bar{f} &= \sigma d\delta - \bar{s}dT + \mu d\Gamma \\ d\bar{\gamma} &= d(\bar{f} - \mu\Gamma) = \sigma d\delta - \bar{s}dT - \Gamma d\mu \end{aligned} \quad (3)$$

where μ is defined by $\partial\bar{f}(\delta, \Gamma, T)/\partial\Gamma$ and is the equilibrating chemical potential of the solute as it is present locally along the interface.

Limiting Thermodynamic Cases of Separation

Within this framework, we may identify two limiting cases of isothermal separation (3,4): The classically considered one is separation at composition equilibrium with bulk phases, *i.e.*, with $\mu = \text{constant}$, for which the work $\int \sigma d\delta$ of interfacial separation is

$$\begin{aligned} (2\gamma_{\text{int}})_{\mu=\text{const.}} &= \bar{\gamma}(\infty, \mu, T) - \bar{\gamma}(\delta_b, \mu, T) \\ &= (2\gamma_{\text{int}})_0 - \int_{-\infty}^{\mu} [2\Gamma_s(\mu') - \Gamma_b(\mu')] d\mu' , \end{aligned} \quad (4)$$

where $\delta = \delta_b(\mu, T)$ on the unstressed boundary. Here $\Gamma = 2\Gamma_s(\mu)$ and $\Gamma = \Gamma_b(\mu)$ describe the relations between Γ and μ at fixed temperature T for the two free surfaces ($\delta = \infty$) created by separation (*i.e.*, $\Gamma_s(\mu)$ is the composition on a single one of the pair) and for the unstressed boundary or interface ($\delta = \delta_b$). Similarly, for separation at constant composition Γ , the work $\int \sigma d\delta$ is

$$\begin{aligned} (2\gamma_{\text{int}})_{\Gamma=\text{const.}} &= \bar{f}(\infty, \Gamma, T) - \bar{f}(\delta_b, \Gamma, T) \\ &= (2\gamma_{\text{int}})_0 - \int_0^{\Gamma} [\mu_b(\Gamma') - \mu_s(\Gamma'/2)] d\Gamma' . \end{aligned} \quad (5)$$

Here, $\delta = \delta_b(\Gamma, T)$ on the unstressed boundary, and $\mu = \mu_s(\Gamma/2)$ and $\mu = \mu_b(\Gamma)$ describe the two relations between Γ and μ mentioned above. Often $(2\gamma_{\text{int}})_0$, which refers to the impurity free interface ($\Gamma = 0$), is written as $2\gamma_s - \gamma_b$.

Detailed forms for the two limiting works of separation defined by eqs. (4) and (5) have been given in the literature (5,6) based on the Langmuir-McLean form,

$$\begin{aligned} \mu_b(\Gamma_b) &= \Delta h_b - T\Delta s_b^\circ + RT \ln[\Gamma_b/(\Gamma_b^\circ - \Gamma_b)] , \\ \mu_s(\Gamma_s) &= \Delta h_s - T\Delta s_s^\circ + RT \ln[\Gamma_s/(\Gamma_s^\circ - \Gamma_s)] . \end{aligned} \quad (6)$$

Here $\Delta s_{b/s}^\circ$ is a vibrational entropy term and $\Gamma_{b/s}^\circ$ denote values of $\Gamma_{b/s}$ at full coverage. Also, $\Delta g_{b/s} = \Delta h_{b/s} - T\Delta s_{b/s}^\circ$ is the free energy of segregation relative to the bulk, where $\mu = RT \ln[x/(1-x)] \approx RT \ln x$ in a bulk phase with fraction x of available sites occupied by the solute.

For isothermal separation at constant composition Γ (below Γ_b°), the entropy terms are generally found to make a small contribution at room temperature (2), and

$$\begin{aligned} (2\gamma_{\text{int}})_{\Gamma=\text{const.}} &\approx (2\gamma_{\text{int}})_0 - (\Delta g_b - \Delta g_s)\Gamma \\ &\approx (2\gamma_{\text{int}})_0 - (\Delta h_b - \Delta h_s)\Gamma \end{aligned} \quad (7)$$

For isothermal separation at constant chemical potential μ , which equilibrates initial coverage Γ on the unstressed boundary,

$$\begin{aligned} (2\gamma_{\text{int}})_{\mu=\text{const.}} &= (2\gamma_{\text{int}})_0 \\ &\quad - RT \left[2\Gamma_s^\circ \ln \left(\frac{\Gamma_b^\circ + (\lambda - 1)\Gamma}{\Gamma_b^\circ - \Gamma} \right) - \Gamma_b^\circ \ln \left(\frac{\Gamma_b^\circ}{\Gamma_b^\circ - \Gamma} \right) \right] \end{aligned} \quad (8)$$

where

$$\lambda = \exp[(\Delta g_b - \Delta g_s)/RT] .$$

Separation at constant μ is always the more embrittling of the two cases discussed, for it may be shown (3,4) that so long as $d\Gamma/d\mu > 0$ on the pair of free surfaces, $2\gamma_{\text{int}}$ for slow separation at constant μ is less than that for fast separation at constant Γ .

It can also be shown (1) that the work of separation at constant Γ along a reversible path is a lower bound to the work of separation along actual (irreversible) paths which have the same initial and final states of the interface and pair of free surfaces. Thus, within the limitation that $\bar{f} = \bar{f}(\delta, \Gamma, T)$ and provides an adequate description of the interface and resulting crack surfaces,

$$W \geq W_{\text{rev}} [= \bar{f}(\infty, \Gamma, T) - \bar{f}(\delta_b, \Gamma, T) \quad \text{at const. } \Gamma] \quad (9)$$

where the right side coincides with equations (5) and (7).

Equations (7) and (8) are convenient forms which clearly show that the difference in segregation free energies, $(\Delta g_b - \Delta g_s)$, and the excess, Γ , residing on the interface are important in determining

the embrittling potential of a solute. Estimates of adsorption free energies, Δg , or enthalpies, Δh , are generally difficult to come by. Wynblatt and Ku (7,8) provide a model to estimate surface adsorption energies which depends primarily on the heats of sublimation of the solute and solvent as well as the heat of mixing. The model gives a reasonable estimate of the surface segregation energy for Cu-Bi (9). In principle, $\Delta g = \Delta h - T\Delta s^\circ$ can be determined from high temperature adsorption isotherms for which the surfaces or boundary are at composition equilibrium with the bulk, and in which AES (most frequently) or RBS techniques are used to estimate Γ_b or Γ_s . For such conditions, the chemical potential of the grain boundary/surface, given by eq. (6), is equated to that for the bulk. The resulting expression,

$$\Gamma/(\Gamma^\circ - \Gamma) = x \exp[\Delta g(T)/RT] \quad (10)$$

may be fitted to high T results to define Δg , and Δh and Δs° are determined separately using $\Delta s^\circ = -d(\Delta g)/dT$. Typically, one assumes that values of Δh and Δs° determined above are independent of T down to room temperature conditions.

Rice and Wang (2) have recently surveyed the literature on such determinations of Δg_b and Δg_s for segregants in Fe. There are considerable uncertainties and some inconsistencies in the data. Also, there are indications that $-\Delta g_s$ for low index crystal surfaces may be much larger than for general polycrystalline surface created by intergranular fracture, at least for P and Sn. Unfortunately, for C only the $-\Delta g_s$ for the low index (100) surface is known, and this might seriously overestimate the polycrystalline value. Their results for C, Sn, P, Sb and S in Fe all reduced to $T = 300$ K, are given as broad, approximate ranges in Table 1; the reader is referred to their paper for further discussion of the data and references. By using results summarized by Hirth (10) for H in Fe, including his estimate for Δh_b in terms the segregation enthalpy of H to a dislocation core, and results of Grabke (11), we have added estimates for H in Fe to the table.

We now use the results summarized in Table 1 to evaluate our formulae for $2\gamma_{\text{int}}$, in particular, for the reduction of $2\gamma_{\text{int}}$ from $(2\gamma_{\text{int}})_0$ due to segregation. The reductions are indicated in particular cases in Tables 2 and 3. To interpret the significance of these

TABLE 1

Free Energies of Segregation, in kJ/mol, for Grain Boundaries and (Polycrystalline) Free Surfaces of Fe, at $T = 300$ K. (Data for C, P, S, Sn and Sb from review by Rice and Wang (2); data for H from review by Hirth (10) and from Grabke (11))

Segregant	$-\Delta g_b$	$-\Delta g_s$
C	50-75	73-85 (*)
Sn	30-35	61-87 (**)
P	32-41	76-80 (**)
Sb	8-25	83-130
S	50-58	165-190
H	65-68	71-109

Note: Δh and Δg at T other than 300 K may be estimated from $\Delta g = \Delta h - T\Delta s^\circ$, with $\Delta s_b^\circ \approx 0.02-0.03$ kJ/mol K and $\Delta s_s^\circ \approx 0-0.03$ kJ/mol K.

* Not available for polycrystal surface; 85 kJ/mol is for (100) crystal surfaces.

** Values reported for low index crystal surfaces are higher: 180 kJ/mol for P and > 200 for Sn.

reductions, note that

$$(2\gamma_{\text{int}})_0 = 2\gamma_s - \gamma_b \approx 2(1.95) - 0.78 \approx 3.1\text{J/m}^2$$

for a Fe boundary, using estimates of γ_s and γ_b from Hirth and Lothe (12).

To represent Γ , consider the grain boundary or free surface as a square grid of sites spaced by distance $b = 2.5 \times 10^{-10}$ m. Then $\Gamma = 1.0/b^2 = 1.6 \times 10^{19}/\text{m}^2 = 2.65 \times 10^{-5}$ mol/m² corresponds to coverage of all grid sites. In Table 2, which shows reductions for separations at constant Γ , from eq. (7) and Table 1, we have used a comparatively low value of $\Gamma = 0.25/b^2$, i.e., one-quarter coverage. This suffices to produce reductions which, for known embrittling segregants such as Sn, P, Sb and S in Fe, are of order 10% to 30% of $(2\gamma_{\text{int}})_0$. The

reduction scales with Γ , so long as $\Gamma < \Gamma_b^\circ$ and one is sensibly in the Langmuir-McLean range. For example, $\Gamma = 0.5/b^2$ leads to reductions of order 20% to 60% of $2\gamma_{\text{int}}$.

TABLE 2

Segregant-induced Reduction in Work of Separation, $2\gamma_{\text{int}}$, in J/m^2 , for Fe Grain Boundaries at $T = 300 \text{ K}$ for Fixed Interfacial Composition, Γ , during Separation. (Results, in J/m^2 , for $\Gamma = 0.25/b^2 = 4 \times 10^{18}/\text{m}^2 = 7 \times 10^{-6} \text{ mol/m}^2$ and $(2\gamma_{\text{int}})_0 = 3.1 \text{ J/m}^2$.)

Segregant	$(2\gamma_{\text{int}})_0 - (2\gamma_{\text{int}})_{\Gamma=\text{const}}$
C	-0.01-0.25(*)
Sn	0.18-0.40
P	0.25-0.34
Sb	0.41-0.85
S	0.75-0.98
H	0.02-0.31

Note: The results scale with Γ ; *e.g.*, reductions are twice as large for $\Gamma = 0.5/b^2$ and half as large for $\Gamma = 0.125/b^2$.

* Based on Δg_s for (100) crystal surface; if $-\Delta g_s$ for polycrystal surface is substantially smaller, as seems to be the case for P and Sn, then negative reductions in $2\gamma_{\text{int}}$ would be predicted. *I.e.*, C segregation would then increase $2\gamma_{\text{int}}$.

These effects are large but segregants can be much more deleterious when there is sufficient solute mobility so that the idealized limit is approached of separation at constant μ , *i.e.*, composition equilibrium with the bulk throughout the separation process. This case is difficult to deal with because simple L-McL adsorption isotherms, using segregation energies as in Table 1, suggest that the pair of free surfaces will usually be fully saturated after separation, *i.e.*, $\Gamma = 2\Gamma_s^\circ$ after separation, unless x is extraordinarily low or T high. In that case the L-McL model becomes inaccurate and segregant interactions, multi-layer coverage, *etc.* should be considered. Nevertheless, using the simple L-McL model, we make estimate for two interesting cases in Table 3.

The first is for high temperature separation in presence of S as a segregant, where there is assumed to be enough mobility for full composition equilibrium with the bulk concentrations indicated during separation. The effects in reducing $2\gamma_{\text{int}}$ are very large. Knott (13) argues that the high temperature stress relief cracking of steels near weld zones may be a consequence of the mobility of S, which then allows (as a high mobility limit) the sort of large reductions of $2\gamma_{\text{int}}$ shown in our table. It may be checked that the grain boundary coverage with S when it is at equilibrium with the bulk phase at the temperature assumed is negligible for the first two x values shown. Thus $2\gamma_{\text{int}}$ would be barely reduced in "fast" separation, at constant $\Gamma [= \Gamma_b(\mu)]$ in those cases but it is seen to be reduced by a large amount for "slow" separation of fixed μ in those same cases.

The second illustration in Table 3 is for H in Fe at 300K. Bulk concentrations and the pressures on a H_2 gas phase with which they are in equilibrium are indicated. Over this broad pressure range, H is seen to substantially reduce $2\gamma_{\text{int}}$ assuming, of course, that it is sufficiently mobile and the fracture process is slow enough for conditions of separation at constant μ to be approached. For the same choice of Δg values, the reduction of $2\gamma_{\text{int}}$ in Table 2, for separation at constant Γ , would be 0.17 J/m^2 with $\Gamma = 0.25/b^2$, and this increases to 0.67 J/m^2 if we make Γ as large as possible, *i.e.*, $\Gamma = \Gamma_b^\circ = 1.0/b^2$ in this illustration. The values in Table 3 for separation at constant μ are much larger and this, again, shows the effect of mobility of the solute in embrittlement.

Some guidelines for characterizing embrittling versus beneficial, and perhaps even cohesion enhancing, segregants emerge from those considerations, assuming that it is proper to focus on the effect of the segregant on $2\gamma_{\text{int}}$ as a key to understanding embrittlement. A deleterious segregant has a large value of the integrands in eqs. (4) and (5). Essentially, this translates by eq. (7) into large values of $\Delta g_b - \Delta g_s$ at the fracture temperature and abundant segregation Γ . True cohesion enhancers should show negative values for the integrands of eqs. (4) and (5), as would be the case for an anomalous segregator which, at a given potential, segregates more to a grain boundary than to a pair of fracture surfaces. *E.g.*, B appears to show such segregation features in Ni_3Al , and it relieves the grain boundary brittleness normally shown in that system (14,15) and thus is probably a true cohesion enhancer. C appears to be a beneficial segregant

TABLE 3

Segregant-induced Reduction in Work of Separation, $2\gamma_{\text{int}}$, for Fe Grain Boundaries for Fixed Equilibrating Potential, μ , during Separation.

<u>S at $T = 900$ K</u>		
$(\Gamma_b^\circ = \Gamma_s^\circ = 0.5/b^2, \Delta g_s = -175 \text{ kJ/mol}, \Delta g_b = -55 \text{ kJ/mol})$		
x_S	$(2\gamma_{\text{int}})_0 - (2\gamma_{\text{int}})_{\mu=\text{const}}$	
10^{-8}	0.96 J/m ²	
10^{-6}	1.86 J/m ²	
10^{-4}	2.73 J/m ²	

<u>H at $T = 300$ K</u>		
$(\Gamma_b^\circ = \Gamma_s^\circ = 1.0/b^2, \Delta g_s = -90 \text{ kJ/mol}, \Delta g_b = -66 \text{ kJ/mol})$		
x_H	$P_{H_2}(\star)$	$(2\gamma_{\text{int}})_0 - (2\gamma_{\text{int}})_{\mu=\text{const}}$
1.94×10^{-9}	0.01 atm	1.71 J/m ²
1.94×10^{-8}	1.0 atm	1.87 J/m ²
1.94×10^{-7}	100 atm	2.02 J/m ²

* Related to x_H , by (Hirth [10]) $1.8 \times 10^{-3} (P/\text{atm})^{1/2} \times \exp(-3440 \text{ K}/T)$, here 1 atm = 10^5 N/m^2 .

in Fe in two ways. First, because it has a relatively high segregation energy to the grain boundary, it tends to displace, by site competition, other more deleterious segregants which may be present there (*e.g.*, 11, 16, 17, 18)). Our results in Tables 1 and 2 suggest that C is, in fact, a modest cohesion degrader, less harmful than, say, P or Sb. On this basis Rice (1) suggested that the entire beneficial effect of C is due to displacement. However, that conclusion may be based on the lack of polycrystalline surface segregation energy data for C; see (2) and footnotes to Tables 1 and 2. It is possible that C might actually lower $2\gamma_{\text{int}}$. In any event, there are convincing experiments (17,18) showing that in addition to the displacement effect by site competition, C has a further beneficial effect which seems to mark it

as a true cohesion enhancer. It is thus unresolved as to whether the effects of C on cohesion are sensibly explained in terms of its effect on $2\gamma_{\text{int}}$.

DISLOCATION EMISSION FROM A CRACK TIP

The Kelly-Tyson-Cottrell and Rice-Thomson approaches have focused on the competition of dislocation emission and atomic decohesion as a fundamental test of whether a given crystal or interface may cleave. An important idea in the Rice-Thomson model and refinements to it is that a critical crack tip loading is required for crack tip dislocation emission. This concept has been supported by experimental observations of loaded crack tips in several f.c.c. and b.c.c. materials (19). We will briefly discuss the features of and reservations in using the model as revised by Mason (20), which compares two local crack tip values of G associated with dislocation emission (G_{disl}) and cleavage-like decohesion ($G_{\text{cleav}} = 2\gamma_{\text{int}}$), or equivalently, the local elastic stress intensity factors $(K_M)_{\text{disl}}$ and $(K_M)_{\text{cleav}}$ for a given loading mode M . In addition to impurity effects on G_{cleav} discussed earlier, impurity segregation to the dislocation core, stacking fault (if a partial), and blunting ledge at the crack tip is predicted to lower G_{disl} .

The geometry for dislocation emission is shown in Fig. 2, where an emergent semicircular dislocation loop of radius r and Burgers vector of magnitude b and direction angle ψ is positioned on a slip plane at angle ϕ . The crack tip is completely contained by the slip plane. The energy to introduce the dislocation loop into a loaded crack tip region is written as (21,22,6,1)

$$U = \pi r [E_{\text{core}} + \alpha b^2 \ln(8mr/e^2 b)] + 2r E_{\text{ledge}} - 3.5br^{3/2} K_M S_M . \quad (11)$$

The last term is the work produced by the crack tip stress field, described by K_M , acting through the slip displacement b ; the preceding term is the energy (E_{ledge} , per unit length) of the crack tip blunting ledge left by the dislocation, and the first two terms with $m = 1$ represent one-half of the total self energy of a full circular loop of radius r in an uncracked, infinite body. The factor m is included to describe the exact elastic interaction between a dislocation loop and a crack; its value depends on ψ and ϕ and is estimated between approximately 1.2 and 2.3 for a representative case of partial

and full dislocation nucleation in f.c.c. crystals and along symmetric tilt interfaces (23,24). In the full circular loop expression, E_{core} is the average energy per unit length contained within a cylinder of radius b of the dislocation line and αb^2 is the average of the pre-logarithmic energy factor over all straight dislocation lines positioned in the loop plane and having Burgers vector b of the loop. Thus, $\alpha = (2 - \nu)\mu/8\pi(1 - \nu) \approx \mu/10$ for an isotropic solid with elastic shear modulus μ . Further, $E_{\text{core}} = \alpha b^2 \ln(b/r_0)$ provides a relation between the familiar dislocation core cutoff r_0 and E_{core} .

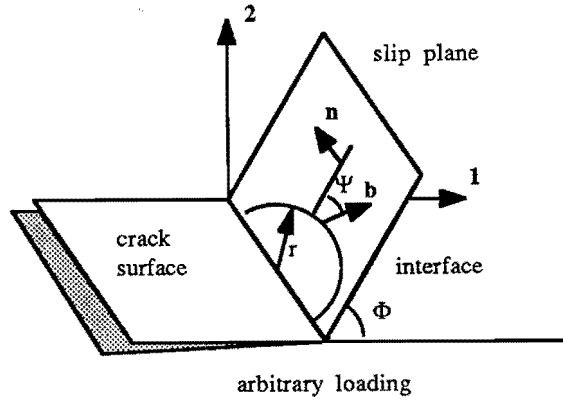


FIG. 2. Geometry for an emergent semicircular loop at a crack tip.

The loop nucleation condition is given by satisfying $dU/dr = 0$ and $d^2U/dr^2 = 0$, and yields

$$(K_M S_M)_{\text{disl}} = \frac{1.2\alpha b^{1/2}}{\sqrt{r/b}}, \quad (12)$$

where the corresponding critical loop radius is

$$r = \frac{e^3}{8m} \exp \left[- \left(\frac{E_{\text{core}}}{\alpha b^2} + \frac{2E_{\text{ledge}}}{\pi \alpha b^2} \right) \right]. \quad (13)$$

The orientation factors S_M are functions of the loading mode M, angles ψ and ϕ , and elastic properties of the materials joining the interface so that $K_M S_M / \sqrt{\rho}$ is the resolved shear traction acting on

the slip plane in the direction of \vec{b} , at a distance ρ from the crack tip. In particular, for a crack in an isotropic body under mode 1 loading,

$$S_1 = \sqrt{1/8\pi} \cos(\phi/2) \sin \phi \cos \psi .$$

Equation (12) describes a planar surface in K -space (25,21) with intercepts $K_M^0 = 1.2ab/\sqrt{r}S_M$ along each axis as shown in Fig. 3. Thus, the critical condition for emission is defined as that point along a given path of local crack tip loading which intersects the planar surface.

The cleavage criterion discussed in the first section of the manuscript and the emission criterion discussed here in terms of K_M are related through

$$G = K_M \Lambda_{MN} K_N , \quad (14)$$

where the components Λ_{MN} used in the summation over $M, N = 1, 2, 3$ above can be determined for cracks in anisotropic single crystals (26) or along crystal interfaces (27), provided the region of oscillatory stresses in the latter is sufficiently small (46, 47). For the intergranular crack in an isotropic material, eq. (14) becomes

$$G = [(1 - \nu)/2\mu](K_1^2 + K_2^2) + (1/2\mu)K_3^2 ,$$

where $\nu =$ Poisson's ratio. If G above is equated to G_{cleav} defined in eq. (1), the cleavage decohesion surface may be drawn as a quadratic surface in Fig. 3, with intercepts of K_1 and K_2 equal to $\sqrt{2\mu G_{\text{cleav}}/(1 - \nu)}$, and K_3 equal to $\sqrt{2\mu G_{\text{cleav}}}$. Equivalently, one may use eq. (14) to calculate G_{disl} and compare it to G_{cleav} , although it is important to note that no unique value of G_{disl} exists for general mixed mode loadings, since the critical condition is a function of $(K_M S_M)_{\text{disl}}$.

There are considerable uncertainties in calculating $(K_M S_M)_{\text{disl}}$ or G_{disl} as outlined, so that results should be taken as suggestive. The emission criterion has only been calculated in the context of linear elasticity, and depends on poorly characterized parameters describing an inherently atomistic structure such as the dislocation core energy, the energy of the dislocated ledge at the loaded crack tip, and configurations of very-near-tip dislocation loops. Often, the critical values of r estimated by eq. (13) are of order one to two Burgers vectors and are well outside the range of continuum elastic dislocation theory. At best, a lower bound to $(K_M S_M)_{\text{disl}}$ can be obtained in such

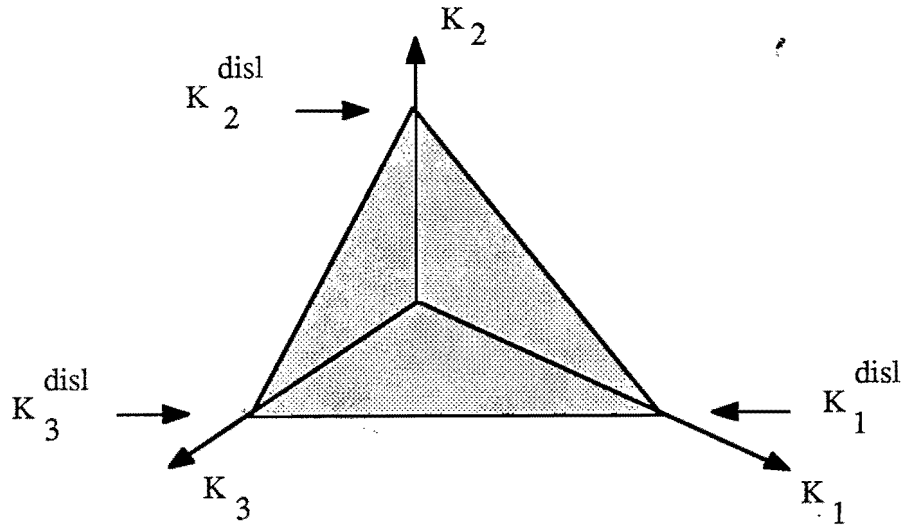


FIG. 3. Graphical representation of eq. (12), showing conditions for dislocation emission in terms of local stress intensity factors.

cases by substituting for r in eq. (12) the smallest value at which a continuum elastic approach is expected to be valid. In addition, the assumed geometry that the crack tip lie completely in a slip plane may favor dislocation emission, since other geometries would require some crack alignment to the slip plane or complicated dislocation loop jogs in order to emit a dislocation. Finally, dislocation loop shapes should be a function of the elastic anisotropy, core and ledge energies, and the local, perhaps mixed crack tip loading; thus, any constraint on shape should in principle overestimate the critical load set, $(K_M S_M)_{\text{disl}}$.

Three final, but important reservations concern the validity of the G_{disl} versus G_{cleav} approach outlined. In many cases of interest, brittle phase nucleation sites (situated perhaps in front of a large, stationary crack) may act as points of injection of rapidly moving cracks into the matrix, and the prediction that a stationary crack emit a dislocation may not be applicable to such a dynamic situation (28). Further, cracks predicted as intrinsically brittle by the criterion proposed may in fact blunt and relax from diffusive plastic flow of nearby dislocations not considered in the analysis. Rate effects, temperature, and current dislocation density (flow stress) may therefore control whether a local energy release G_{cleav} may exist at the crack tip (29,30). Finally, experimental work of Vehoff, Neumann,

and coworkers (31-34) questions the assumption that a crack tip responds in a distinctly ductile or brittle manner. Here, the sharpness of a fatigue loaded crack tip in Fe-3% Si single crystals is seen to vary significantly with temperature, loading rate, and environmental H. The interpretation is that continuously varying levels of cleavage crack extension and ductile crack opening due to dislocation slip are contributing to the crack tip opening angle.

Effects of Impurity Segregation on $(K_M S_M)_{\text{disl}}$

The effect of a solute on the reversible work to nucleate a dislocation is discussed for conditions of chemical equilibrium. The result is used to consider changes in the critical load set, $(K_M S_M)_{\text{disl}}$ in eq. (12), for dislocation nucleation due to a rapidly mobile impurity such as H in Fe.

Consider a body at pressure P and temperature T from which we may adsorb/desorb a solute and in which we may form dislocations. A reversible change in the internal energy of the body is given by

$$dU = TdS - PdV + \mu_H dn_H + e d\ell \quad , \quad (15)$$

where n_H and μ_H are the number and chemical potential of the solute atoms (denoted here by 'H' for application to hydrogen) in the system, and e is the free energy per unit length of dislocation formed. Analogous to surface or grain boundary free energy, e is the reversible work required to effect unit increase in dislocation line length, and we assume $e = e(\mu_H, P, T, \ell)$ in general, with a simpler model being e independent of ℓ . This representation is an approximation, in that not all energy changes associated with alteration of dislocation line positions and introduction of new dislocations can be described by such a parameterization.

For conditions where a dislocation of length $d\ell$ is introduced into the body at constant P, T and $\mu_H = \mu_0$, it is convenient to define the following state variable

$$d\Lambda = d(U + PV - TS - \mu_H n_H) = -SdT + VdP - n_H d\mu_H + e d\ell \quad .$$

Therefore, the reversible work to enlarge the total dislocation length by $d\ell$ at constant P, T , and $\mu_H = \mu_0$ is given by

$$e = \left(\frac{\partial \Lambda}{\partial \ell} \right)_{P, T, \mu_H} = \left(\frac{\partial G}{\partial \ell} \right)_{P, T, \mu_H} - \mu_0 \Gamma(P, T, \mu_0, \ell) \quad ,$$

where $\Gamma = (\partial n_H / \partial \ell)_{P,T,\mu_H}$ is defined as the excess number of solute atoms associated with a unit length of dislocation. From the expression for Λ , we may obtain the following Maxwell relation,

$$\left(\frac{\partial e}{\partial \mu_H} \right)_{P,T,\ell} = - \left(\frac{\partial n_H}{\partial \ell} \right)_{P,T,\mu_H} = -\Gamma(P, T, \mu_H, \ell) .$$

The above equation may be integrated along a path of constant P , T , ℓ from $\mu = -\infty$ (corresponding to absence of solute in the system) to $\mu_H = \mu_0$,

$$e_H = e_0 - \int_{-\infty}^{\mu_0} \Gamma(\mu_H) d\mu_H . \quad (16)$$

Thus, the reversible work of forming a unit length of dislocation in the presence of a solute is given above, with e_0 equal to the work of formation in the absence of solute.

Equation (16) is evaluated for conditions where the dislocation is formed at chemical equilibrium between the solute and the bulk and dislocation core sites. A McLean isotherm (see eq. (10)) is used to define the equilibrium excess Γ_d at the dislocation in terms of the lattice concentration x , the segregation free energy Δg_d to the dislocation sites, and the saturation excess level Γ_d^0 at the dislocation. Since the solute is assumed to be dilute in the lattice, $(d\mu_H)_{P,T} = RT dx/x$, and eq. (16) is evaluated as

$$e_H = e_0 - RT\Gamma_d^0 \ln[1 + x \exp(-\Delta g_d/RT)] . \quad (17)$$

The fact that chemical equilibrium is assumed between the bulk and dislocation allows e_H to be expressed directly in terms of x .

The same treatment may be applied to the dislocation ledge, or the stacking fault left by a partial, assuming that the free energies of each are dependent only on P , T , and μ_H . In such cases, E_{core} and E_{ledge} appearing in the criterion for emission of a full loop dislocation (see eq. (12)) may be replaced by using eq. (17). The critical condition for nucleation would be given in terms of the pure system value, thus

$$\begin{aligned} (K_M S_M)_H &= (K_M S_M)_0 \\ &\times [1 + x \exp(-\Delta g_d/RT)]^{-RT\Gamma_d^0/2\alpha b^2} \\ &\times [1 + x \exp(-\Delta g_{\text{ledge}}/RT)]^{-RT\Gamma_{\text{ledge}}^0/2\alpha b^2} \end{aligned} \quad (18)$$

where subscripts 'd' and 'ledge' denote quantities evaluated for the dislocation and ledge, respectively. For conditions where the dislocation core and ledge act as segregation sites (*i.e.*, $\Delta g_d, \Delta g_{ledge} < 0$), the effect of adding an impurity to the bulk material is seen to reduce the critical load set, $(K_M S_M)_{disl}$, for dislocation emission. This effect is intended to complement impurity effects on atomic decohesion discussed earlier, and on diffuse plastic flow from external, non-crack-tip dislocations as discussed by Hirth for H in Fe (10). The effect of H on dislocation emission in Fe is difficult to estimate, since Γ_d^0 and Γ_{ledge}^0 are poorly known. For comparison, the binding energy of H to a nonscrew dislocation in Fe is estimated as -58.6 kJ/mol (35), which is considerably lower than either the estimate of -95 kJ/mol for a carbide interface (36) or -104 kJ/mol for a Fe (110) surface (37).

Another possible effect of impurity segregation, not considered here, is that large-atomic-size segregants may retain some residual misfit even after segregation along the grain boundary. A first analysis (38) suggests that this may impede dislocation nucleation at the tip.

APPLICATION TO Cu-Bi INTERFACIAL CRACKS

The Prediction of the Model

Earlier work by Wang *et al.* (6) has outlined theoretical estimates of G_{cleav} and G_{disl} for mode 1 cracks on Cu-Bi [110] symmetrical tilt interfaces. The resulting estimates predict strong differences in G_{cleav} and G_{disl} which depend on the particular crystallographic interface, the crack growth direction, and the amount of Bi segregated to the interface. The closing section of this manuscript reports on experimental observations of fracture surface morphology in mode 1 tested Cu-Bi bicrystals, in an effort to determine how useful and fundamental is the G_{cleav} versus G_{disl} approach outlined.

Here we give improved estimates for the critical G values of Wang *et al.* (6). Their work was based on an approximate estimate (21,22) of the correction factor m for dislocation self energy, of eq. (11); here we use the results of subsequent exact continuum elastic calculations (23). Also, the grain boundary segregation energy, $-\Delta g_b$, for the $\Sigma 11$ boundary was overestimated in their work (9).

Using 3-D weight functions, Gao and Rice (23) derived the self

energy of a crack-tip dislocation loop and computed the energy correction factor m as a function of ϕ and ψ . Computations showed that for a semicircular loop $m(\phi, \psi)$ decreases monotonously with increasing ϕ and this angular dependence is the strongest at $\psi = 0^\circ$ and becomes weaker as ψ increases. Since G_{disl} is scaled by a factor of m for a mode 1 loading, using new values of m modifies the orientation dependence of G_{disl} .

The misorientation and structural dependence for grain boundary segregation has been the subject of wide interest in recent years and a variety of results, sometimes contradictory, have been published. In spite of inconsistencies of data from different laboratories, experimental results (24,39) and theoretical analysis (40,41) suggest that segregation to $\Sigma 11$ $[110]/(1\bar{1}3)$ boundaries is very unlikely. The value of Δg_b used by Wang *et al.* (6) is an overestimate and a much lower value was estimated by Wang (24). This leads to a stronger misorientation dependence of the effect of Bi content on G_{cleav} . Combining corrections for the values of m and the values of $-\Delta g_b$ for the $\Sigma 11$ $[110]/(1\bar{1}3)$, $\Sigma 9$ $[110]/(2\bar{2}1)$ and $\Sigma 41$ $[110]/(4\bar{4}3)$ boundaries, Wang (24) recently recalculated G_{cleav} and G_{disl} for model 1 cracks on Cu-Bi $[110]$ symmetrical tilt boundaries.

The estimates reported in Wang (24) are shown in Fig. 4 which displays G_{cleav} and G_{disl} for three representative grain boundaries, with crack growth in either $[n\bar{n}\bar{m}]$ (denoted by (+)) or $[\bar{n}nm]$ (denoted by (-)) opposing directions as to contain the crack front completely in a $\{111\}$ slip plane as required by the model. The solid black line then divides cleavage and ductile behavior into two regions based on $G_{\text{cleav}} > G_{\text{disl}}$ and $G_{\text{cleav}} < G_{\text{disl}}$, respectively.

Estimates for a pure boundary at room temperature are shown in Fig. 4 by the rightmost point on a given horizontal line, and the effect of Bi segregation is to move leftward, reducing $2\gamma_{\text{int}} [= G_{\text{cleav}}]$. G_{disl} is assumed to be unaffected by the immobile Bi, and is shown here for the nucleation of two partials on the $\{111\}$ planes symmetrically disposed about the interface rather than for the full (undissociated) loop as described earlier. The partial calculation is similar, and is outlined in detail by Anderson (21) and Wang *et al.* (6). In particular, the energy U_1 associated with nucleation of the first partial is written as for U in eq. (11), except now a term $\pi r^2 \gamma_{\text{sf}}/2$ is added to account for the energy of the stacking fault. For the mode 1 loading discussed here, the first partial is found to expand to a stable radius of order

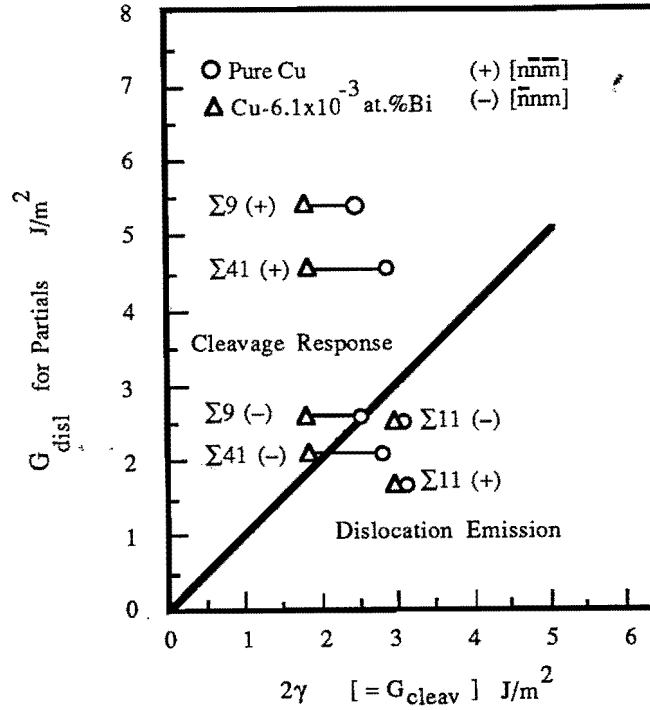


FIG. 4. Predictions of cleavage and partial dislocation emission for interfacial cracks on three representative Cu-Bi [110] symmetric tilt boundaries. The effect of Bi segregation is to move the prediction for a given crack geometry leftward on the horizontal lines shown. (+) and (-) denote opposite crack growth direction on a boundary.

100*b* to 1000*b* due to the dominance of the stacking fault term at large *r*. The energy U_2 of the second partial is written as U in eq. (11), with an added term $-\pi r^2 \gamma_{sf}/2$ to account for the removal of the stacking fault, and an added interaction energy between the first and second partials. The calculation yields $(K_1)_{disl}$ values for the first and second partials which bound that for nucleation of the full dislocation in a given orientation. Even though the calculation predicts a lower load to nucleate the full dislocation than the partials, the latter is regarded as more plausible since once the first partial is nucleated, the possibility of a full, undissociated loop is unlikely. There are considerable uncertainties involved in the estimate of core and ledge energies which are discussed along with the other parameter choices needed for G_{disl} in (21).

Predictions of G_{cleav} are based on separation at constant Γ so

that eq. (7) is applicable. A more complete discussion of appropriate parameter choices to apply eq. (7) to Cu-Bi interfaces is found in (9,21,24). The Bi concentration, Γ , residing on the interface is estimated assuming equilibration of the interface and bulk solute at the annealing temperature, $T_a = 723$ K. Thus, eq. (10) is used to calculate Γ for the bulk (lattice) concentration of $x = 6.1 \times 10^{-3}$ at. %, estimating $\Gamma_b^\circ = 3.41 \times 10^{-5}$ mol/m² and taking $\Delta g_b = -67.6$ kJ/mol, -56.6 kJ/mol and -42.8 kJ/mol for the $\Sigma 41$, $\Sigma 9$ and $\Sigma 11$ boundaries, respectively (24). Values of $(2\gamma_{\text{int}})_0$ are based on the free energy difference, $2\gamma_a - \gamma_b$, between two clean free surfaces and the clean grain boundary, and are predicted to vary by up to 20% due primarily to variation of γ_b with orientation (21).

Several features are seen from Fig. 4: 1. Grain boundary orientation is important in determining the nature of crack tip response, due to variations in $2\gamma_{\text{int}}$ and G_{disl} . The $\Sigma 11$ boundary is most ductile, because its low grain boundary free energy and segregation energy and the orientation of the slip planes at the crack tip are favorable for dislocation emission. The strong dependence on slip plane orientation causes the difference in G_{disl} among the three boundaries to be more significant if the crack propagates in the $[n\bar{n}\bar{m}]$ direction. 2. Segregation of Bi to the boundary reduces $2\gamma_{\text{int}}$ and hence embrittles the $\Sigma 9$ and $\Sigma 41$ boundaries. The $\Sigma 11$ boundary is not embrittled by Bi segregation due to a smaller segregation energy. Decreases in $2\gamma_{\text{int}}$ are in the range of 5% and 35% when $x = 6.1 \times 10^{-3}$ at. %, depending on the grain boundary. 3. The direction of the crack propagation strongly affects the ductile versus brittle response because of the difference in the resolved shear stress acting on the active slip plane. The difference is large for $\Sigma 41$ and $\Sigma 9$ boundaries, so that the bicrystals are predicted to be ductile when the crack grows in along one direction, and become brittle if the crack propagates in another direction. In cases where the crack tip is not coplanar with a slip plane, crack propagation may tend to a cleavage mode.

Experimental Results

In order to check the prediction of the model, two symmetrical $[110]$ tilt grain boundaries, $\Sigma 11[110]/(1\bar{1}3)$ and $\Sigma 9[110]/(2\bar{2}1)$, were studied. As a comparison, one symmetrical $[100]$ tilt grain boundary, $\Sigma 5[100]/(031)$, and one asymmetrical random grain boundary were also studied. The bicrystals were grown by the vertical Bridge-

man technique. The bulk concentration is believed to be lower than 100 ppm (0.003 at. %) Bi except for the $\Sigma 5$ bicrystal. Different heat treatments were applied. The notches were made along grain boundaries. Specimens were fractured and the fracture surfaces were compared. The detailed experimental procedure and results were described elsewhere (24) and the experimental results are summarized as follows.

The $\Sigma 11$ bicrystal is essentially ductile after any heat treatment. After annealing at 723 K or 773 K in vacuum the specimen could not be broken by bending. The surface newly created by bending at the near tip region is shown in Fig. 5, which is a so called tearing topography surface (42) and the appearance of this type of fracture surface indicates an excellent ductility. Doping with Bi by annealing the specimen in Bi vapor did not reduce the ductility notably, but occasionally small areas of the faceted boundary could be found on the background of the tearing topography surface (Fig. 6). The bicrystal was slightly embrittled by annealing in the liquid Bi bath for a long time. After this treatment, a mixed fracture surface appeared with the major area still being transgranular and small areas of intergranular fracture along the faceted interface as shown in Fig. 7. These results indicate that the $\Sigma 11$ boundary is highly resistant to Bi segregation and embrittlement.

The $\Sigma 9$ grain boundary is also ductile after the segregation treatment by annealing at 723 or 773 K in vacuum. From the ease of breaking the specimen by bending, its ductility is lower than $\Sigma 11$. By annealing in Bi vapor, the $\Sigma 9$ boundary was severely embrittled. A faceted quasi-cleavage topography surface appeared in the curved area of the boundary (Fig. 8). The detailed discussion (24,43) showed that this type of faceted structure consists of three mutually perpendicular crystallographic planes which are 2 sets of $\{110\}$ type planes and 1 set of serrated $\{100\}$ type planes. The appearance of this type of fracture surface seems to be related to a special type of intergranular brittle fracture where the cracking path is apparently not coincident with the boundary plane at the microscopic level. Rather it may wander along the boundary by cleavage of $\{110\}$ plane and dislocation slip, which produces the serration of $\{100\}$ planes.

The random grain boundary studied is usually brittle after annealing at 723 or 773 K in vacuum. When the annealing temperature was low (723 K) so that grain boundary faceting did not occur, a



FIG. 5. The tearing topography surface of the $\Sigma 11$ bicrystal. (723 K in vacuum for 96 hours)

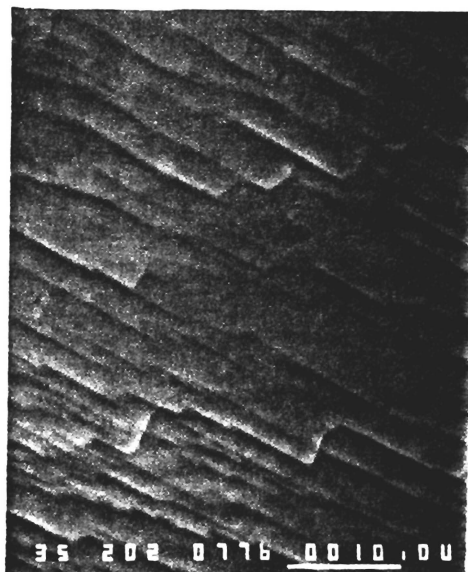


Fig. 6. The small faceted fracture area of the $\Sigma 11$ bicrystal. (1123 K, 24 hrs. + 773 K, 24 hrs in Bi vapor)

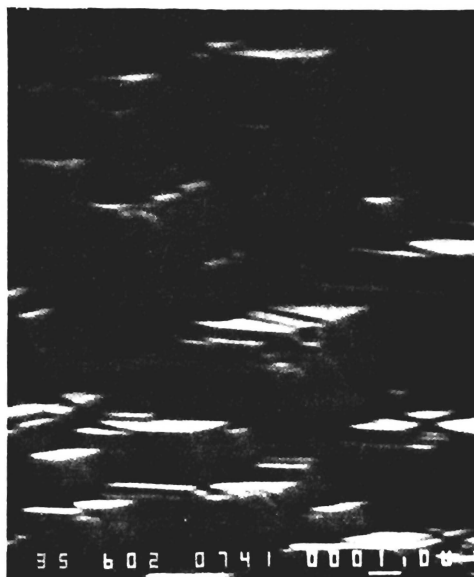


FIG. 7. The small faceted fracture area of the $\Sigma 11$ bicrystal. (1123 K 24 hrs + 723 K, 96 hrs in Bi bath)

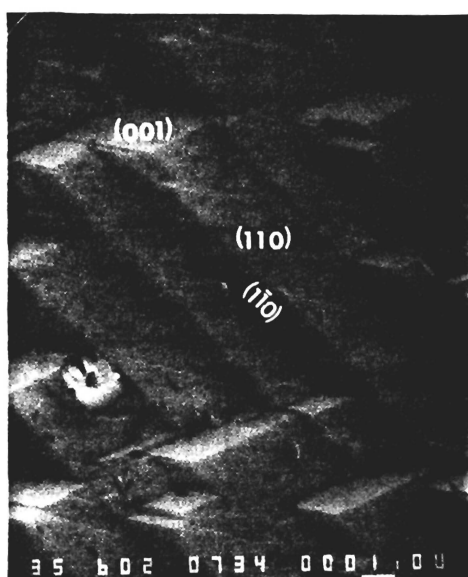


FIG. 8. The faceted quasi-cleavage topography surface of the $\Sigma 9$ bicrystal. (1123 K 24 hrs + 723 K 96 hrs. in Bi vapor)

curved boundary fractured in a brittle manner producing the faceted quasi-cleavage topography surface (Fig. 9). At higher annealing temperature (773 K) the curved grain boundary was faceted, resulting in a faceted intergranular fracture surface (Fig. 10) with the elongated facet direction along the un-curved direction and regular steps that accommodate the macroscopic curvature. In contrast for a planar boundary annealed at higher temperature (773 K), only small scale faceting occurred and resulted in a mixed fracture surface with neither the large scale faceting nor faceted quasi-cleavage topography surface.

The $\Sigma 5$ grain boundary is brittle in the as-grown condition. A thermal contraction crack formed along the interface during solidification and cool-down of the bicrystal. The crack was readily propagated under a tensile load, leading to a very low ductility and a variety of brittle fracture surfaces, which are composed of the faceted quasi-cleavage topography surface (Fig. 11), the large scale faceted intergranular fracture surface and also the relatively flat fine scale faceted intergranular fracture surface (Fig. 12).

The experimental results are consistent with the theoretical predictions in Fig. 4 that the $\Sigma 11$ grain boundary is ductile and it cannot be embrittled by segregation regardless of the cracking direction and the heat treatment. The $\Sigma 9$ bicrystal could not be embrittled by segregation but it was severely embrittled by doping with Bi. This is, to some extent, consistent with the prediction in Fig. 4 when cracking is in the $[\bar{1}14]$ direction, considering that the bulk concentration of the bicrystal is lower.

The model can only deal with the situation that the crack front is situated in a potentially active slip plane. This geometry seems to provide the most favorable condition for dislocation emission. For any other geometries dislocation emission is expected to be more difficult. The brittle behaviors of the $\Sigma 5$ and the random grain boundaries are thus compatible with this framework. On the other hand, propensities of Bi segregation in the $\Sigma 5$ and the random grain boundaries are expected to be large from the consideration of the excess volume of the boundary plane (44) or from the newly suggested argument that the most important geometrical parameter governing the behavior of special interfaces is the interface spacing of the lattice planes parallel to the interface plane (45). The reduced decohesion energy of the interface combining with the difficulty in dislocation emission leads to low ductilities of the $\Sigma 5$ and the random boundaries.

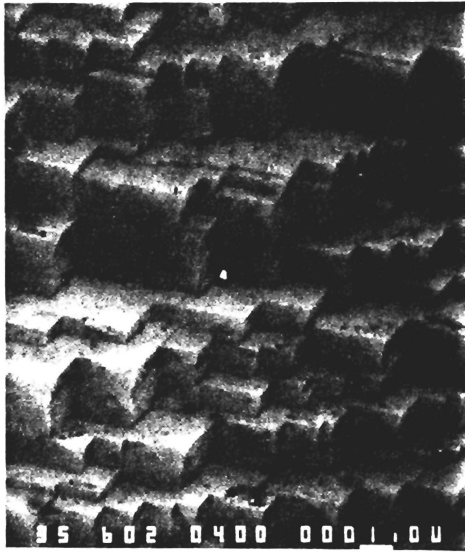


FIG. 9. The faceted quasi-cleavage topography surface of the random boundary. (723 K, 96 hrs. in vacuum)

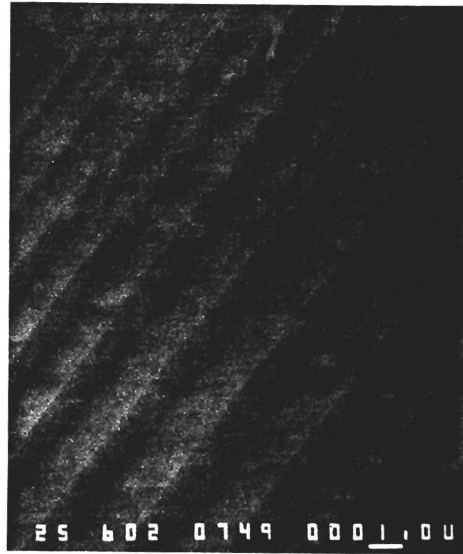


FIG. 10. The faceted intergranular fracture surface of the random boundary. (773 K 24 hrs in vacuum)

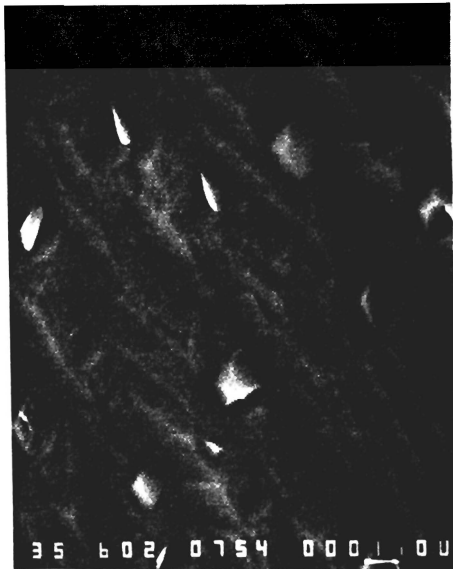


Fig. 11. The faceted quasi-cleavage topography surface of the $\Sigma 5$ bicrystal. (as-grown)



FIG. 12. The fine scale faceted intergranular fracture surface of the $\Sigma 5$ bicrystal. (as-grown)

An important prediction of the model is that the ductile versus brittle response of an interfacial crack depends on the cracking direction, and in some cases, *e.g.* for the $\Sigma 9$ boundary, the dependence may be very strong. This prediction was verified indirectly by tests on a what was supposed to be 'pure' Cu $\Sigma 9$ bicrystal. A fatigue strain hardened specimen cut from this bicrystal was sectioned to form two specimens and notches were cut along the interfaces in opposite directions. One was in the $[\bar{1}\bar{1}\bar{4}]$ direction, the other in $[\bar{1}14]$. The two notched specimens were fatigue tested again. It turned out that the fracture behaviors of the two specimens are completely different. The one with the $[\bar{1}\bar{1}\bar{4}]$ direction notch fractured at a lower load in fewer cycles and the fracture surface appeared to be brittle intergranular. The one with the $[\bar{1}14]$ direction notch fractured at a much higher load in a large number of cycles and the fracture surface was transgranular with well developed fatigue striations. We cannot take this test as full evidence for the model prediction because a large number of sulphides were found on the fracture surface of the brittle specimen, and these particles might be the source of the brittleness. Thus, we can not be certain from this test whether the $\Sigma 9$ boundary in pure Cu is ductile or brittle when cracking in the $[\bar{1}14]$ direction. But the result is compatible with the theoretical prediction in the sense that the only difference between the two specimens is the cracking direction, and their response is significantly different.

SUMMARY DISCUSSION

We have presented thermodynamic and mechanical models of interfacial embrittlement, illustrating results with applications to various segregants (H, C, P, Sn, Sb, S) on Fe grain boundaries, and have described studies of Cu bicrystals with Bi segregation as a model system to test theoretical concepts.

The thermodynamic formulation for interfacial decohesion in presence of a segregating species relates the work of separation, $2\gamma_{\text{int}}$, to segregation free energies at the grain boundary (Δg_b) and pair of surfaces (Δg_s) created by fracture. Separation in presence of a mobile segregant, which can allow approach to idealized limiting conditions of separation at constant equilibrating potential of the segregant, leads to substantial reductions in $2\gamma_{\text{int}}$, as shown for H and S in Fe. The more typical case at low temperatures, of separation at fixed composition, leads to smaller but still significant reductions of

$2\gamma_{\text{int}}$, illustrated for various segregants in Fe.

Segregants which decrease $2\gamma_{\text{int}}$, and thus presumably embrittle grain boundaries, have relatively large values of $\Delta g_b - \Delta g_s$ and sit with abundant coverage Γ at the boundary. Those which increase $2\gamma_{\text{int}}$, and are presumably true cohesion enhancers, have negative values of $\Delta g_b - \Delta g_s$ as is apparently the case for B in Ni_3Al . A segregant can be beneficial, however, so long as it simply does not have a large value of $\Delta g_b - \Delta g_s$ and acts to displace other more deleterious segregants from the boundary. Such displacement is to be expected if $-\Delta g_b$ is large, because then the segregant wins out over others by site competition. C in Fe is beneficial partly because it has a high $-\Delta g_b$ and displaces other deleterious elements from the boundary. It also seems to have an additional beneficial effect, but estimates based on currently available surface segregation data suggest that it modestly decreases, rather than increases, $2\gamma_{\text{int}}$. This conclusion may, however, change if segregation energy data becomes available for C segregation to the general polycrystal surfaces of intergranular fractures, rather than just to a (100) crystal surface as at present.

Updates of the Rice-Thomson formalism were outlined for addressing the competition between cleavage decohesion and blunting by dislocation emission for atomistically sharp cracks along interfaces. This is to determine if an interface is intrinsically cleavable for a given direction of cracking along it. As we discuss, factors relating to the presence and mobility of nearby dislocations (and hence to loading rate and temperature) will often control whether an interface, judged as intrinsically cleavable, will actually fail by cleavage.

Aspects of the modelling discussed here include more exact estimates by continuum elasticity of the self-energy of dislocation loops emerging from a crack tip, the possibility of nucleation in a partial dislocation mode, and effects of a mobile solute, notably H, which could segregate along an emerging loop.

The theory for the dislocation emission versus cleavage competition is applied to a model system of Cu bicrystals, symmetrically tilted about [110], on the boundary of which Bi may segregate. Detailed results are given for the $\Sigma 11/(1\bar{1}3)$ and $\Sigma 9/(2\bar{2}1)$ boundaries, and predict that the latter is more readily affected by Bi and is more brittle. A dependence of load levels for dislocation nucleation on the direction of crack growth is found in the case of the $\Sigma 9[110]/(2\bar{2}1)$

boundary. This relates to different orientations of potentially relaxing slip systems relative to the crack tip.

In coordinated experiments, several Cu-Bi bicrystals were grown, heat treated for segregation, and tested mechanically. These include the two $[110]$ tilt cases just mentioned and also the $\Sigma 5[100]/(031)$ symmetrical tilt boundary and a high angle random grain boundary. Results for the two $[110]$ tilt cases have qualitative consistency with the theoretical predictions, although the theory is probably inadequate to explain all results and could not be checked with much precision due to factors relating to nearby dislocations and uncontrolled impurities. Consistent with the theory, the $\Sigma 9[110]/(2\bar{2}1)$ bicrystal is readily embrittled with Bi whereas the $\Sigma 11[110]/(1\bar{1}3)$ remains ductile. Also, the $\Sigma 9$ bicrystal showed brittle interfacial fracture for one direction of crack growth but a highly ductile failure mode for the opposite direction.

In order of brittleness, the Cu-Bi bicrystals are $\Sigma 5[100]/(031)$, random, $\Sigma 9[110]/(2\bar{2}1)$ and $\Sigma 11[110]/(1\bar{1}3)$. The fracture surface morphologies are highly varied, often from place to place along the same boundary. Brittle intergranular fracture surfaces may have large planar areas, or be highly faceted. Sometimes the facets reflect interfacial faceting, as it thought to be induced by Bi segregation, but in other cases they seem to show a new type of interfacial brittle failure in which the crack path may not microscopically follow the boundary and forms flat cleavage like $\{110\}$ facets and also $\{100\}$ facets which sometimes show slip markings.

ACKNOWLEDGEMENT

This study was supported by the NSF Materials Research Laboratory at Harvard.

REFERENCES

1. J. R. Rice, in *Chemistry and Physics of Fracture* (R. M. Latani- sion and R.H. Jones, eds.) (Martinus Nijhoff Publishers, Dor- drecht, 1987) p. 27.
2. J.R. Rice and J.-S. Wang, "Interfacial embrittlement by solute segregation", submitted to *Mater. Sci. Eng.*, 1988.

3. J. R. Rice, in *Effect of Hydrogen on Behavior of Metals* (A. M. Thompson and I. M. Bernstein, eds.) (TMS-AIME, New York, 1976) p. 455.
4. J. P. Hirth and J. R. Rice, *Metall. Trans.* **11A**, 1502 (1980).
5. R. J. Asaro, *Phil. Trans. Roy. Soc. London* **A295**, 150 (1980).
6. J.-S. Wang, P.M. Anderson, and J.R. Rice, in *Mechanical Behaviour of Materials - V* (M.G. Yan, S.H. Zhang and Z.M. Zheng, eds.) (Pergamon Press, Oxford, 1987) p. 191.
7. P. Wynblatt and R. C. Ku, *Surface Sci.* **65**, 511 (1977).
8. P. Wynblatt and R. C. Ku, in *Interfacial Segregation* (W. C. Johnson and J. M. Blakely, eds.) (ASM, Metals Park, OH, 1979) p. 115.
9. J.-S. Wang, "Review of Data to Evaluate Segregation Effects on the Ductile-Brittle Transition in Cu-Bi Bicrystals," Harvard University, Informal Progress Report (unpublished), 1985.
10. J. P. Hirth, *Metall. Trans. A* **11A**, 861 (1980).
11. H. J. Grabke, *Steel Research* **57**, 178 (1986).
12. J. P. Hirth and J. Lothe, *Theory of Dislocations*, (McGraw-Hill, New York, 1968).
13. J. F. Knott, in *Chemistry and Physics of Fracture* (R. M. Lantianision and R. H. Jones, eds.) (Martinus Hijhoff Publishers, Dordrecht, 1987) p. 44.
14. C. T. Liu, C. L. White and J. A. Horton, *Acta Metall.* **33**, 213 (1985).
15. C. L. White, *J. Vac. Sci. Technol.* **A4**, 1633 (1986).
16. H. J. Grabke, in *Chemistry and Physics of Fracture*, (R.M. Lantianision and R. H. Jones eds.) (Martinus Nijhoff Publishers, Dordrecht, 1987), p. 388.
17. S. Suzuki, M. Obata, K. Abiko and H. Kamura, *Trans. Iron Steel Inst. Jap.* **25**, 62 (1985).
18. S. Suzuki, S. Tanii, K. Abiko and H. Kimura, *Metall. Trans.* **18A**, 1109 (1987).
19. S. M. Ohr, *Mater. Sci. Eng.* **72**, 1 (1985).
20. D. D. Mason, *Phil. Mag.* **39**, 455 (1979).
21. P. Anderson, "Ductile and Brittle Crack Tip Response" (Ph.D. Dissertation, Harvard University, 1986).
22. P. M. Anderson and J. R. Rice, *J. Mech. Phys. Solids* **35**, 743 (1987).
23. H. Gao and J. R. Rice, *J. Mech. Phys. Solids*, in press.

24. J.-S. Wang, "Fracture Surfaces of Embrittled f.c.c. Metal Bicrystals and their Misorientation Dependence," to be submitted to *Acta Metall.*
25. I. H. Lin and R. Thomson, *Acta metall.* **34**, 187 (1986).
26. P. C. Paris and G. C. Sih, in *Fracture Toughness Testing and its Applications*, (ASTM Spec. Tech. Publ. 381), (1965) p. 30.
27. J. R. Willis, *J. Mech. Phys. Solids* **19**, 353 (1971).
28. M. L. Jokl, V. Vitek, and C. J. McMahon Jr., *Acta metall.* **28**, 1479 (1980).
29. L. B. Freund and J. W. Hutchinson, *J. Mech. Phys. Solids* **33**, 169 (1985).
30. L. B. Freund, J. W. Hutchinson, and P. S. Lam, *Eng. Fracture Mech.* **23**, 119 (1986).
31. H. Vehoff and P. Neumann, *Acta metall.* **27**, 915 (1979).
32. H. Vehoff and P. Neumann, *Acta metall.* **28**, 265 (1980).
33. H. Vehoff, W. Rothe, and P. Neumann, in *Fracture 1981*, vol. 1 ICF5. Cannes (1981), p. 265.
34. H. Vehoff and W. Rothe, *Acta metall.* **11**, 1781 (1983).
35. A. J. Kunnick and H. H. Johnson, *Acta metall.* **28**, 33 (1980).
36. J. P. Hirth and H. H. Johnson, in *Atomistics of Fracture* (R. M. Latanision and J. R. Pickens, eds.) (Plenum Press, New York, 1983) p. 771.
37. K. Christmann, in *Atomistics of Fracture* (R. M. Latanision and J. R. Pickens, eds.) (Plenum Press, New York, 1983) p. 363.
38. J. Yu and J. R. Rice, in *Interfacial Structure, Properties and Design*, (M. H. Yoo, C. L. Briant and W. A. T. Clark, eds.), Mat. Res. Soc., vol. 122, (1988), in press.
39. J.-S. Wang, in *Interfacial Structure, Properties and Design*, (M. H. Yoo, C. L. Briant and W. A. T. Clark eds.), Mat. Res. Soc. vol. 122, (1988), in press.
40. D. Bouchet and L. Priester, *Scripta Metall.* **21**, 475 (1987).
41. V. Paidar, *Acta Metall.* **35**, 2035 (1987).
42. Metal Handbook, 9th edition, vol. 12, ASM, Metal Park, OH (1987) p. 21.
43. J.-S. Wang, *J. Mater. Res.* **3**, 16 (1988).
44. H. J. Frost, M. F. Ashby, and F. Spaepen, "A Catalogue of [100], [110] and [111] Symmetric Tilt Boundaries in Face-centered Cubic Hard-Sphere Crystals," MRL Technical Report, Harvard University (1982).

45. D. Wolf, in *Electronic Packaging Materials Science*, (E. A. Griess, K. N. Tue, and D. R. Uhlmann, eds.) (Mat. Res. Soc. vol. 40, 1985,) p. 341.
46. J. R. Rice, *J. Appl. Mech.* **55**, 98 (1988).
47. P. M. Anderson, "Small-Scale Contact Conditions for the Linear Elastic Interface Crack," to appear in *J. Appl. Mech.* (1988).